ChemComm

COMMUNICATION

View Article Online
View Journal | View Issue

Cite this: *Chem. Commun.*, 2024, **60**, 7586

Received 22nd May 2024,
Accepted 20th June 2024

DOI: 10.1039/d4cc02483d

rsc.li/chemcomm

Oxidation mechanism of phenols by copper(II)–halide complexes†

Lan Yang, Rin Ito, Hideki Sugimoto, Yuma Morimoto and Shinobu Itoh *

The mechanism of oxidation of phenols by tetrahedral copper(II)–halide complexes was investigated to demonstrate that phenols with an electron-withdrawing substituent are oxidized *via* a proton-transfer/electron-transfer (PTET) mechanism, whereas phenols with an electron-donating substituent involve a concerted proton/electron transfer (CPET) mechanism. The importance of the tetrahedral geometry of the metal centre as well as the effects of the halide ligands of the substrates were explored.

The redox reactivity of transition-metal complexes depends largely on the geometry of the metal centre. In the case of copper(II) complexes with similar donor groups, for example, the oxidation ability of copper(II) complexes taking a tetrahedral (Td) geometry may be higher than those having a square planar, square pyramidal, or trigonal bipyramidal structure, since the Td geometry is more suited to the copper(I) oxidation state compared to the others. To explore the redox reactivity of such tetrahedral copper(II) complexes, we have developed a series of copper(II) complexes, $[Cu^{II}(TMG_3tach)X]^+$ ($\mathbf{1^X}$), where TMG_3tach is an N_3-tridentate ligand consisting of *cis,cis*-1,3,5-triaminocyclohexane (tach) and *N*,*N*,*N*′,*N*′-tetramethylguanidino (TMG) substituents, and X is an anionic co-ligand (F^-, Cl^-, Br^-, I^-, MeO^-, $C_6F_5O^-$, $C_6F_5S^-$, or ROO^-).[1–3] Reactivity studies of the halide complexes demonstrated that they undergo Cu^{II}–X bond cleavage, and in the case of X = F^-, Cl^-, and Br^-, they induce C–H bond activation of an external substrate, such as 1,4-cyclohexadiene (CHD) with a weak C–H bond (76.0 ± 1.2 kcal mol^{-1}),[4] to give the corresponding copper(I) complex and benzene as the oxidation product.[3] Such C–H bond activation reactivity of transition-metal halide complexes has been reported by using high-valent transition-metal halide complexes of Ni^{III}, Pd^{IV}, Cu^{III}, and Au^{III}, where the higher oxidation state of the metal ions induces homolytic cleavage of the metal–halide bond.[5–14] In the case of $\mathbf{1^X}$, on the other hand, the metal centre has a normal Cu^{II} oxidation state, but not a high-valent metal ion such as Cu^{III}. Thus, we suspected that such reactivity of halide complexes can be attributed to their tetrahedrally distorted geometry, which induces Cu^{II}–X bond homolysis to give Cu^{I} and $X^{\bullet}$, the latter of which formally abstracts a hydrogen atom from the substrate.[3] Unfortunately, however, the oxidation reaction of CHD by $\mathbf{1^X}$ was too slow to perform a detailed kinetic analysis.

In this study, we further examined the reactivity of $\mathbf{1^X}$ (X = F^-, Cl^-, Br^-, or I^-) toward phenolic substrates (4-substituted-2,6-di-*tert*-butylphenol $\mathbf{P^YH}$, Scheme 1) in order to shed light on the O–H bond activation mechanism by copper(II)–halide complexes. Phenols are often used as a mechanistic probe for hydrogen atom transfer reactions. To examine the geometric effect on the reactivity of copper(II)–halide complexes, we also employed copper(II)–halide complexes $\mathbf{2^X}$ (X = Cl^- or Br^-) supported by a tripodal tetradentate ligand TMG_3tren (1,1,1-tris(2-(N^2-(1,1,3,3-tetramethylguanidino))ethyl)amine),[15–17] that enforces the trigonal bipyramidal (Tbp) geometry of the metal centre (Fig. 1).

Fig. 2(a) shows the spectral changes observed upon the addition of $\mathbf{P^{tBu}H}$ (Y = *tert*-butyl, 12.5 mM) to $\mathbf{1^{Br}}$ (0.25 mM) in CH_3CN at 0 °C under an N_2 atmosphere as a typical example, where the absorption bands at 410 and 560 nm due to $\mathbf{1^{Br}}$ gradually decrease with a concomitant increase in the absorption bands at 380, 400 and 626 nm, obeying first-order kinetics (see the first-order plot shown in the inset to Fig. 2(a)). The absorption bands of the post-reaction solution at 380, 400 and 626 nm are identical to those of

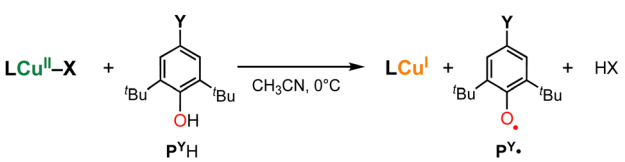

Scheme 1 Reaction of copper(II)–halide complexes and 4-substituted-2,6-di-*tert*-butylphenol ($\mathbf{P^YH}$).

Department of Molecular Chemistry, Division of Applied Chemistry, Graduate School of Engineering, Osaka University, 2-1 Yamada-oka, Suita, Osaka 565-0871, Japan. E-mail: shinobu@chem.eng.osaka-u.ac.jp

† Electronic supplementary information (ESI) available: Experimental procedures, kinetic analysis data, EPR and MALDI-TOF mass spectra of the post-reaction solutions and 19F-NMR for the detection of HF. See DOI: https://doi.org/10.1039/d4cc02483d

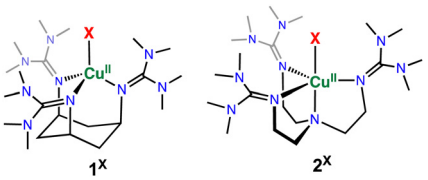

Fig. 1 ChemDraw structures of $\mathbf{1}^{X}$ and $\mathbf{2}^{X}$.

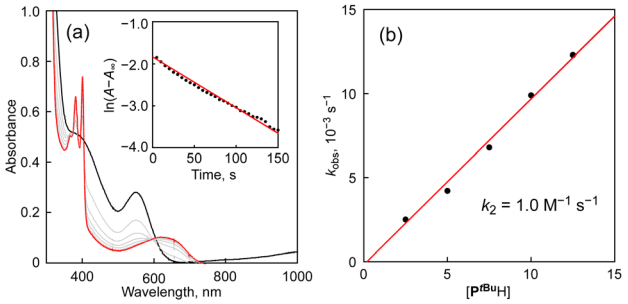

Fig. 2 (a) UV-vis spectral changes for the reaction of $\mathbf{1}^{Br}$ (0.25 mM) with 2,4,6-tri-*tert*-butylphenol ($\mathbf{P}^{tBu}$H, 12.5 mM) in CH_3CN at 0 °C. Inset: A pseudo-first-order plot based on the absorption change at 410 nm. (b) Plot of k_{obs} *vs.* substrate concentration.

the 2,4,6-tri-*tert*-butylphenoxyl radical ($\mathbf{P}^{tBu\bullet}$), and its quantitative formation based on $\mathbf{1}^{Br}$ was confirmed using the reported ε values of $\mathbf{P}^{tBu\bullet}$.[18] The formation of the phenoxyl radical $\mathbf{P}^{tBu\bullet}$ and the copper(I) complex was further confirmed by the EPR spectrum shown in Fig. S1 (ESI†), where only an EPR signal ascribable to $\mathbf{P}^{tBu\bullet}$ was observed at g = 2.0041,[19] but the EPR signals due to the copper(II) complex $\mathbf{1}^{Br}$ completely disappeared. The fate of the generated HBr will be discussed below.

The pseudo-first-order rate constant (k_{obs}) obtained from the plot of $\ln(A - A_\infty)$ against the reaction time (inset of Fig. 2(a)) showed linear correlation with the concentration of $\mathbf{P}^{tBu}$H, as shown in Fig. 2(b), from which the second-order rate constant (k_2) was determined to be 1.0 M^{-1} s^{-1} from the slope.

Importantly, both $\mathbf{2}^{Cl}$ and $\mathbf{2}^{Br}$ taking a Tbp geometry did not show such reactivity toward $\mathbf{P}^{tBu}$H under the same reaction conditions, clearly demonstrating that the Td geometry of the metal centre is crucial to inducing O–H bond activation reactivity.

Then, the reactions of $\mathbf{1}^{Br}$ and a series of phenol derivatives $\mathbf{P}^{Y}$H (Y = OMe, Et, H, CHO, or COMe) were examined under the same reaction conditions (in CH_3CN at 0 °C) to gain an insight into the mechanism of the phenol oxidation reaction. The kinetic analysis data are given in Fig. S2–S6 (ESI†). In all cases except $\mathbf{P}^{COMe}$H, the reaction obeyed first-order kinetics in the presence of an excess amount of $\mathbf{P}^{Y}$H (a pseudo-first-order reaction condition) and plots of the observed first-order rate constants (k_{obs}) against the substrate concentration exhibited linear correlation, from which the second-order rate constants (k_2) were determined from the slopes. For $\mathbf{P}^{COMe}$H, the second-order rate constant (k_2) was determined in the presence of a stoichiometric amount of the substrate (under a second-order reaction condition, Fig. S6, ESI†). In the case of $\mathbf{P}^{OMe}$H as the

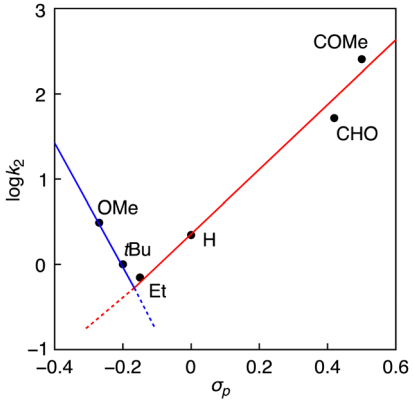

Fig. 3 Hammett plot for the reaction of $\mathbf{1}^{Br}$ and $\mathbf{P}^{Y}$H.

substrate, the quantitative formation of the phenoxyl radical product $\mathbf{P}^{OMe\bullet}$ was also confirmed by the appearance of its characteristic absorption bands at 387, 406 and 542 nm (Fig. S3, ESI†).[20] On the other hand, the final organic product of the reactions with other phenols $\mathbf{P}^{Y}$H (Y = Et, H, CHO, or COMe) were confirmed to be 3,3′,5,5′-tetra-*tert*-butyl-[1,1′-bi(cyclohexylidene)]-2,2′,5,5′-tetraene-4,4′-dione by MALDI-TOF mass spectra, as shown in Fig. S7 (ESI†), which was formed by the C–C coupling reaction of the generated phenoxyl radical species $\mathbf{P}^{Y\bullet}$ and the subsequent elimination of Y_2 from the dimeric intermediate (Scheme S1, ESI†).[10]

Fig. 3 shows a Hammett plot of $\log k_2$ against σ_p. As can clearly be seen, the reaction rate (k_2) increases linearly as the electron-withdrawing (EW) ability of the *p*-substituent Y increases (increasing the σ_p value) in going from Y = Et to COMe with a Hammett ρ value of 4.0. In the cases of **Y** = OMe or *t*Bu, however, the data points deviated from the linear line, where the reaction rates were larger than those expected from the linear correlation. Such a phenomenon was also observed in the reactions of phenol derivatives with copper(III)-superoxide (Cu^{III}–$OO^{\bullet}$) and nickel(III)–fluoride (Ni^{III}–F) complexes supported by 2,6-diamidepyridine ligands.[10,21] The authors suggested a change of reaction mechanism across the series of phenol derivatives. Namely, the reactions where the phenols have an electron-withdrawing (EW) substituent involve a PTET (proton transfer following electron transfer) mechanism, whereas the oxidation of phenols with an electron-donating (ED) substituent includes a hydrogen atom transfer (HAT) or concerted proton/electron transfer (CPET) mechanism. Kinetic deuterium isotope effects (KIEs) were determined to be 1.6 and 1.7 for the oxidation of $\mathbf{P}^{OMe}$H(D) and $\mathbf{P}^{tBu}$H(D), respectively (Fig. S8 and S9, ESI†). Such a small KIE value was reported in the oxidation of $\mathbf{P}^{H}$H by an Ni^{III}–Cl complex supported by a 2,6-diamidepyridine ligand, for which the CPET mechanism was proposed.[9] On the other hand, no kinetic deuterium isotope effect was observed (KIE = 1.0) in the oxidation of $\mathbf{P}^{COMe}$H(D) with an EW-substituent by $\mathbf{1}^{Br}$ (Fig. S10, ESI†).

To explain these kinetic results, we propose the reaction mechanism illustrated in Scheme 2.

For phenol substrates with an EW-substituent, such as $\mathbf{P}^{COMe}$H, deprotonation of the phenol substrate by one of the

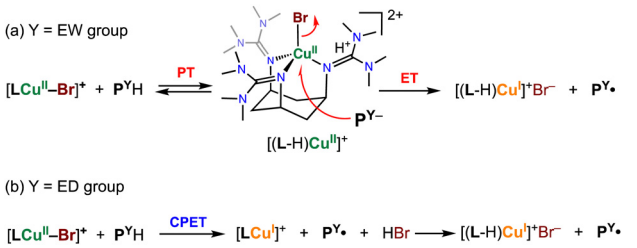

Scheme 2 Proposed mechanism for the phenol oxidation reaction by $\mathbf{1}^{\mathbf{X}}$.

TMG substituents of the supporting ligand takes place, causing an acid–base equilibrium (initial PT process in Scheme 2(a)). Then, electron transfer from the generated phenolate to copper(II) ion occurs concomitantly with dissociation of Br^-, giving a copper(I) complex and the phenoxyl radical product $\mathbf{P}^{\mathbf{COMe}\bullet}$. Dissociated Br^- forms a guanidinium salt with the protonated TMG substituent (Scheme 2(a)). Thus, the reductive dissociation process of Br^- from the Cu^{II}–Br centre is rate-limiting. This mechanism is consistent with the fact that no KIE was observed, as mentioned above.

On the other hand, for the reaction of phenols with an ED-substituent, like $\mathbf{P}^{\mathbf{OMe}}$H, such a proton transfer from the phenol hardly occurs due to the higher pK_a of the phenolic proton of $\mathbf{P}^{\mathbf{OMe}}$H, so that concerted proton/electron transfer (CPET) becomes the major pathway (Scheme 2(b)). In this case as well, the generated HBr eventually forms a guanidinium salt with the TMG substituent of the supporting ligand (Scheme 2(b)).

To gain further insight into the reaction mechanism, the effects of the halide ligands **X** were examined using $\mathbf{P}^{\mathbf{COMe}}$H with EW-substituents as substrates under the same reaction conditions. Fig. S12–S14 (ESI†) show the kinetic analysis data for the reactions of $\mathbf{1}^{\mathbf{F}}$, $\mathbf{1}^{\mathbf{Cl}}$, and $\mathbf{1}^{\mathbf{I}}$, respectively. The k_2 values for these reactions were determined in the presence of a stoichiometric amount of the substrate (a second-order reaction condition), since the reactions of $\mathbf{P}^{\mathbf{COMe}}$ were too fast under the pseudo-first-order reaction conditions (in the presence of an excess amount of the substrate). Thus, the plot of $(A_0 - A)/[\mathrm{Cu}]_0(A - A_\infty)$ against time gave a straight line passing through the origin, from which the second-order rate constant (k_2) was obtained as the slope of the linear line, as listed in Table 1. Reported Cu–X bond dissociation energy (BDE) values are also included in Table 1 and the plot of $\log k_2$ against the BDE of Cu–X is shown in Fig. 4.

Notably, the $\log k_2$ of $\mathbf{1}^{\mathbf{I}}$, $\mathbf{1}^{\mathbf{Br}}$ and $\mathbf{I}^{\mathbf{Cl}}$ exhibited very good linear correlation with the reported BDE values[4] of Cu–X, where the weaker the Cu–X bond, the faster the reaction rate. This is consistent with the proposed mechanism involving the rate-limiting reductive Cu–X dissociation reaction for the oxidation of $\mathbf{P}^{\mathbf{COMe}}$H.

Table 1 The second-order reaction rates (k_2) for the reactions of $\mathbf{1}^{\mathbf{X}}$ and $\mathbf{P}^{\mathbf{COMe}}$H and the reported BDE of Cu^{II}–X

	F	Cl	Br	I
$k_2/10^2$ (M^{-1} s^{-1})	1.25	0.50	2.53	10.34
BDE (kcal mol^{-1}) of Cu–X[4]	103	90	80	70

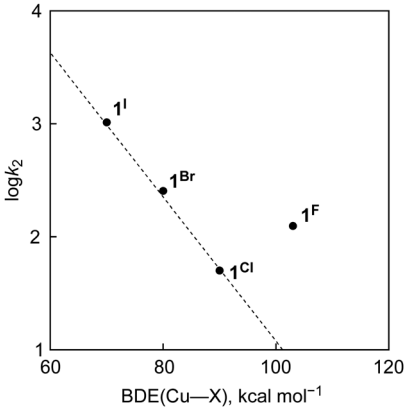

Fig. 4 Plot of $\log k_2$ *vs.* $\mathrm{BDE}_{\mathrm{Cu-X}}$ for the reaction of $\mathbf{1}^{\mathbf{X}}$ and $\mathbf{P}^{\mathbf{COMe}}$H.

On the other hand, the $\log k_2$ value of $\mathbf{1}^{\mathbf{F}}$ is significantly larger than that predicted from the linear line, as shown in Fig. 4. This result clearly indicates that the reaction mechanism of $\mathbf{1}^{\mathbf{F}}$ is different from that of the other complexes ($\mathbf{1}^{\mathbf{I}}$, $\mathbf{1}^{\mathbf{Br}}$, or $\mathbf{I}^{\mathbf{Cl}}$). That is, the oxidation of the phenol by $\mathbf{1}^{\mathbf{F}}$ may involve a CPET mechanism rather than a PTET mechanism. This may be due to the extremely strong BDE of HF (136 kcal mol^{-1})[4] compared to those of the others (HCl: 103 kcal mol^{-1}, HBr: 88 kcal mol^{-1}, HI: 71 kcal mol^{-1}).[4] In fact, we obtained a KIE value of 1.4, similar to those of the CPET reactions mentioned above (KIE = 1.6–1.7, Fig. S11, ESI†). The formation of free HF was confirmed by ^{19}F-NMR for the reaction of $\mathbf{1}^{\mathbf{F}}$ with $\mathbf{P}^{\mathbf{COMe}}$H in CH_3CN (*vide infra*), where the fluorine signal of HF was detected at δ = −148 ppm and its yield was estimated as 78% based on the copper(II) complex using OTf^- as an internal standard (Fig. S15, ESI†).

In summary, we have demonstrated that tetrahedrally distorted copper(II)–halide complexes $\mathbf{1}^{\mathbf{X}}$ supported by a TMG_3tach ligand showed oxidation ability toward phenol derivatives, where substrates with an EW-substituent are oxidized *via* a proton-transfer/electron-transfer (PTET) mechanism and those with an ED-substituent undergo a concerted proton/electron transfer (CPET) mechanism. The importance of the tetrahedral geometry of the metal centre was also demonstrated by comparing the reactivity with that of a copper(II)–halide complex $\mathbf{2}^{\mathbf{X}}$ with a trigonal bipyramidal geometry. Moreover, the TMG group is shown to work as a proton acceptor from the phenol substrate in the PTET mechanism, and in the reaction of $\mathbf{P}^{\mathbf{COMe}}$ and $\mathbf{1}^{\mathbf{F}}$, the strong BDE of HF (the product) greatly enhanced the reactivity. Further mechanistic studies are being conducted to gain more detailed insights into the reaction mechanism.

This work was supported by JST-CREST (JPMJCR16P1 to SI), Grant in Aid for Scientific Research (B) (JSPS 23K26669 to SI) and JST SPRING (JPMJSP2138 to YL).

Data availability

The data supporting this article have been included as part of the ESI.†

Conflicts of interest

There are no conflicts to declare.

Notes and references

1 I. Shimizu, Y. Morimoto, D. Faltermeier, M. Kerscher, S. Paria, T. Abe, H. Sugimoto, N. Fujieda, K. Asano, T. Suzuki, P. Comba and S. Itoh, *Inorg. Chem.*, 2017, **56**, 9634–9645.
2 I. Shimizu, Y. Morimoto, G. Velmurugan, T. Gupta, S. Paria, T. Ohta, H. Sugimoto, T. Ogura, P. Comba and S. Itoh, *Chem. – Eur. J.*, 2019, **25**, 11157–11165.
3 Y. Lan, Y. Morimoto, I. Shimizu, H. Sugimoto and S. Itoh, *Inorg. Chem.*, 2023, **62**, 10539–10547.
4 Y.-R. Luo, *Conprehensive Handbook of Chemical Bond Energy*, CRC Press, Boca Raton, London, New York, 2007.
5 M. H. Pérez-Temprano, J. M. Racowski, J. W. Kampf and M. S. Sanford, *J. Am. Chem. Soc.*, 2014, **136**, 4097–4100.
6 S. J. Hwang, D. C. Powers, A. G. Maher, B. L. Anderson, R. G. Hadt, S.-L. Zheng, Y.-S. Chen and D. G. Nocera, *J. Am. Chem. Soc.*, 2015, **137**, 6472–6475.
7 S. J. Hwang, B. L. Anderson, D. C. Powers, A. G. Maher, R. G. Hadt and D. G. Nocera, *Organometallics*, 2015, **34**, 4766–4774.
8 B. J. Shields and A. G. Doyle, *J. Am. Chem. Soc.*, 2016, **138**, 12719–12722.
9 P. Mondal, P. Pirovano, A. Das, E. R. Farquhar and A. R. McDonald, *J. Am. Chem. Soc.*, 2018, **140**, 1834–1841.
10 P. Mondal and A. R. McDonald, *Chem. – Eur. J.*, 2020, **26**, 10083–10089.
11 D. Gygi, M. I. Gonzalez, S. J. Hwang, K. T. Xia, Y. Qin, E. J. Johnson, F. Gygi, Y.-S. Chen and D. G. Nocera, *J. Am. Chem. Soc.*, 2021, **143**, 6060–6064.
12 S. K. Kariofillis and A. G. Doyle, *Acc. Chem. Res.*, 2021, **54**, 988–1000.
13 J. K. Bower, A. D. Cypcar, B. Henriquez, S. C. E. Stieber and S. Zhang, *J. Am. Chem. Soc.*, 2020, **142**, 8514–8521.
14 M. Lovisari, R. Gericke, B. Twamley and A. R. McDonald, *Inorg. Chem.*, 2021, **60**, 15610–15616.
15 K. W. Krockert, F. Garg, J. Heck, M. V. Heinz, J. Lange, R. Schmidt, A. Hoffmann and S. Herres-Pawlis, *Dalton Trans.*, 2024, **53**, 2973–2990.
16 V. Raab, J. Kipke, O. Burghaus and J. Sundermeyer, *Inorg. Chem.*, 2001, **40**, 6964–6971.
17 H. Wittmann, V. Raab, A. Schorm, J. Plackmeyer and J. Sundermeyer, *Eur. J. Inorg. Chem.*, 2001, 1937–1948.
18 V. W. Manner, T. F. Markle, J. H. Freudenthal, J. P. Roth and J. M. Mayer, *Chem. Commun.*, 2008, 256–258.
19 D. Ar, A. F. R. Kilpatrick, B. Cula, C. Herwig and C. Limberg, *Inorg. Chem.*, 2021, **60**, 13844–13853.
20 J. P. Collman, R. A. Decréau and C. J. Sunderland, *Chem. Commun.*, 2006, 3894–3896.
21 W. D. Bailey, D. Dhar, A. C. Cramblitt and W. B. Tolman, *J. Am. Chem. Soc.*, 2019, **141**, 5470–5480.